An enhanced fast fundamental frequency estimator for three-phase electric aircraft grid

Jula, Bhumaiah ; Jarial, Raj Kumar ; Verma, Anant Kumar; Roncero-Sánchez, Pedro ; Guerrero, Joseph M. ; Busarello, Tiago Davi Curi ; Ahmed, Hafiz

Measurement

DOI:
https://doi.org/10.1016/j.measurement.2022.111142

Published: 15/06/2022

Peer reviewed version

An Enhanced Fast Fundamental Frequency Estimator for Three-Phase Electric Aircraft Grid

Bhumaiah Jula[a], Raj Kumar Jarial[a], Anant Kumar Verma[a], Pedro Roncero-Sánchez[b], Josep M. Guerrero[c], Tiago Davi Curo Bursello[d] and Hafiz Ahmed[e]

[a]National Institute of Technology Hamirpur, Electrical Engineering Department, Hamirpur 177005, Himachal Pradesh, India
[b]Universidad de Castilla-La Mancha, Spain, E.T.S. Ingeniería Industrial De C. Real, Avenida Camilo José Cela S/N, Ciudad Real 13071, Spain
[c]Aalborg University, Denmark, Villum Investigator AAU Energy. The Villum Center for Research on Microgrids (AAU CROM), Copenhagen 9100, Denmark
[d]Federal University of Santa Catarina, Department of Control, Automation and Computing Engineering, Blumenau 89036-256, Brazil
[e]Bangor University, Nuclear Futures Institute, Bangor LL57 1UT, Gwynedd, United Kingdom

ARTICLE INFO

Keywords:
Digital signal processing,
electric aircraft,
frequency estimation,
three-phase grid voltage

ABSTRACT

This article proposes a robust and enhanced three-phase fundamental frequency estimation algorithm for the electric aircraft grid. Unlike conventional frequency-locked loops, the digital signal processing technique-based frequency estimator proposed relies on the storage of five consecutive samples of the fundamental grid voltage signal. Furthermore, the ability to successfully operate at a low sampling frequency, i.e. 8 kHz, makes it sufficiently attractive as regards reducing the memory storage in a low-cost real-time controller. The proposed frequency estimator can additionally eliminate the negative effects of the DC-offset and the fundamental negative sequence components present in the grid signal without any additional effort. Also, the tuning efforts are reduced for the frequency variation range of 350-900 Hz owing to the existence of a single tuning gain parameter. The proposed algorithm has also been found to have a fast dynamic response, which has been experimentally validated through the use of a real-time digital controller.

1. Introduction

The evolution of reliable electronic power technology has, over time, led to numerous changes in the mechanical and electrical systems of conventional aircraft [1]. The term “electrical aircraft (EA)" emerged on the basis of several aspects, such as less consumption of petroleum-based fuels, a reduction in the weight and size of electronic circuits, improved energy-efficient systems, and the possible involvement of renewable energy sources such as solar photovoltaic panels, etc. [2]. Nevertheless, the key components employed in order to strengthen the power system network of an EA consist principally of power conversion circuits, such as DC-DC converters (i.e. buck, boost, etc.) and AC-DC converters (i.e. inverters) [3]. The active power filters employed to improve the power quality of the network also rely on inverters, which are connected to an EA power grid [4]. An EA power system network is, in general, a variable frequency system [5], and the control objective of a power electronic converter may, therefore, become challenging in the supply frequency variation range of 350-900 Hz [4], [5].

Literature contains several examples of control solutions for constant frequency electric aircraft power system networks [6] [7]. The most prominent control algorithms are phase-locked loops (PLLs) [8] and frequency-locked loops (FLLs) [9]. The design of PLLs is quite a lot simpler than that of FLLs, signifying that PLLs are the most popular choice when synchronizing power converters with the grid. The narrow operating range of frequency, i.e. 47-52 Hz [10], in utility networks, has also made it possible to deploy PLLs in order to obtain the frequency information successfully. PLLs are easily implemented in the synchronous reference frame, i.e. the $dq-$frame, but are tedious to tune [11], [12]. In the case of a three-phase power system networks, PLLs may fail to operate properly in the presence of fundamental negative sequence (FNS) and DC-offset components in the grid signal [13] as they will induce second harmonic oscillations and full-cycle oscillations in the $dq-$frame, thus yielding an inaccurate frequency estimation. Several pre-filtering techniques [13], [14], along with an instantaneous symmetrical component method [15], can be applied in order to estimate the fundamental positive sequence (FPS) component and to reject the negative effect of DC-offset such that a narrow bandwidth PLL is obtained, thus improving the dynamic tracking performance of a PLL [16]. However, with the tedious controller tuning approaches, there is always a trade-off between the dynamic response behaviour and the filtering capability [17].

Several control techniques were investigated for their application to EA, such as a discrete Fourier transform (DFT) based PLL [18], a steady-state linear Kalman filter (SSLKF)-PLL [19]-[22], a complex least mean square (CLMS) [23], a sliding mode observer (SMO) [24], an adaptive observer (AO) [25],[26], and a repetitive dual observer (RDO) based PLL [27]-[29]. The DFT-PLL and SSLKF-PLL schemes were found to be computationally more complex, and the frequency tracking abilities of the SSLKF based PLL were better than the those of the DFT based PLL [22]. Despite the superior performance of the SSLKF, better disturbance rejection abilities are still being researched owing to the limitations of the control bandwdith of the SSLKF-PLL.

ORCID(s):

Another approach is that of applying a mean square error minimisation strategy in order to estimate the grid frequency of an EA, which is known as “CLMS". The major drawback of the CLMS is its incapability to handle the grid voltage imbalance [23]. Non-linear observer based techniques such as SMO [23] and ADO [25] could, therefore, help to obtain dynamically stable and simple structure estimation schemes. Unfortunately, neither technique is capable of handling the DC-offset component present in the grid voltage signal. An improved AO based solution is proposed in [26], but it has a slower dynamic response in the presence of harmonics, leading to steady-state errors in the estimated parameters.

Bearing the aforementioned techniques in mind, a non-linear repetitive observer (RO) with which to estimate the frequency of an EA grid is , therefore, introduced [27], and its first control application is that of estimating the rotor angle of a permanent magnet synchronous machine for torque ripple reduction [28]. Nevertheless, a detailed investigation has revealed that the RO is combined with a Kalman filter, leading to a dual observer scheme [29]. It consequently understood that the main objective of an additional RO is to enhance the disturbance rejection abilities of the SSLKF-PLL. Moreover, there is no significant improvement to the dynamic response behaviour of the RDO-PLL when compared to SSLKF-PLL.

Apart from the aforementioned issues, the research into a rapid and robust frequency estimation technique is still actively progressing under large frequency variation, i.e. 350-900 Hz, in order to expand the control horizon. A non-linear FLL (N-FLL) technique with an improved dynamic response and good immunity to grid disturbances was reported in [31]. There is, however, a trade-off between the dynamic response time and the disturbance rejection ability owing to the involvement of various tuning parameters. The N-FLL is sensitive to the DC-offset and the FNS components present in the grid signal, and additional efforts are, therefore, required in order to eliminate the DC-offset component and acquire the FPS for proper operation. In the proposed work, the frequency estimation algorithm is made immune to the DC-offset and the FNS components without any great effort. The tuning approach helps to obtain the fast frequency information at a low sampling frequency. Also, the proposed algorithm does not have any specific feasible frequency range. The frequency range chosen covers the generic range, i.e., 360-800 Hz, in an electric aircraft. Hence, the proposed algorithm can be applied outside of the generic frequency range. The organization of the article is as follows: The proposed fundamental frequency estimator and its features are discussed in Section 2. The detailed experimental investigations are presented in Section 3. Finally, a brief summary of the article is discussed in Section 4.

2. Proposed Fundamental Frequency Detector

This section discusses a simple and computationally efficient three-phase fundamental frequency estimator, which relies on the storage of five consecutive samples of the grid voltage signal. The implementation block diagram of the proposed frequency estimator is exemplified in Fig. 1. For a clear understanding, let us consider a three-phase grid voltage signal as expressed below:

$$\begin{aligned} v_a(k) &= A_1 \cos(\omega_a\, k\, T_s + \phi) \\ v_b(k) &= A_1 \cos(\omega_a\, k\, T_s + \phi - 2\pi/3) \\ v_c(k) &= A_1 \cos(\omega_a\, k\, T_s + \phi + 2\pi/3) \end{aligned} \tag{1}$$

where A_1, ω_a, k, ϕ and T_s are the fundamental amplitude, the angular grid frequency, the current sampling instant, the initial phase angle of the grid voltage and the sampling period, respectively. A three-phase voltage signal can generally be decoupled through the use of Clarke's transformation ($[T_{\alpha\beta}]$) as follows:

$$\begin{bmatrix} v_\alpha(k) \\ v_\beta(k) \end{bmatrix} = \left[T_{\alpha\beta}\right] \begin{bmatrix} v_a(k) \\ v_b(k) \\ v_c(k) \end{bmatrix}; \left[T_{\alpha\beta}\right] = \frac{2}{3} \begin{bmatrix} 1 & -\frac{1}{2} & -\frac{1}{2} \\ 0 & \frac{\sqrt{3}}{2} & -\frac{\sqrt{3}}{2} \end{bmatrix} \tag{2}$$

The decoupled signals are expressed as follows:

$$v_\alpha(k) = A_1\ \cos\left(k\, \omega_a\, T_s\ +\ \phi\right) \tag{3}$$

$$v_\beta(k) = A_1\ \sin\left(k\, \omega_a\, T_s\ +\ \phi\right) \tag{4}$$

where, v_α and v_β are the equivalent orthogonal signals obtained from (1). The intermediate signals for the proposed fundamental frequency estimator shown in Appendix A are, in the case of the $\alpha-$axis component, expressed as follows:

$$L_{1\alpha} = v_\alpha^2(k) - v_\alpha(k)\, v_\alpha(k-4) \tag{5}$$

$$L_{2\alpha} = v_\alpha(k)\, v_\alpha(k-1) - v_\alpha(k)\, v_\alpha(k-3) \tag{6}$$

The intermediate signals for the $\beta-$axis are similarly:

$$L_{1\beta} = v_\beta^2(k) - v_\beta(k)\, v_\beta(k-4) \tag{7}$$

$$L_{2\beta} = v_\beta(k)\, v_\beta(k-1) - v_\beta(k)\, v_\beta(k-3) \tag{8}$$

The variables denoted as L_1 and L_2 help to obtain the frequency estimation law as follows:

$$L_1 = L_{1\alpha} + L_{1\beta} \tag{9}$$

$$L_2 = L_{2\alpha} + L_{2\beta} \tag{10}$$

The frequency estimation law is expressed as follows:

$$L_1 = 2\, L_2\ \cos(\omega_a T_s) \tag{11}$$

In order achieve a more robust solution, a linear regression model of (11) is arranged as follows:

$$\underbrace{L_2}_{x(t)} - \underbrace{2\, L_2}_{\theta(t)} \underbrace{\cos(\,\omega_a\, T_s)}_{\rho} = 0 \tag{12}$$

The fundamental frequency information can consequently be obtained from the unknown parameter ρ by applying the gradient method [30], as follows:

$$\dot{\hat{\rho}} = \xi\, \theta(t)(x(t) - \theta(t)\hat{\rho}) \tag{13}$$

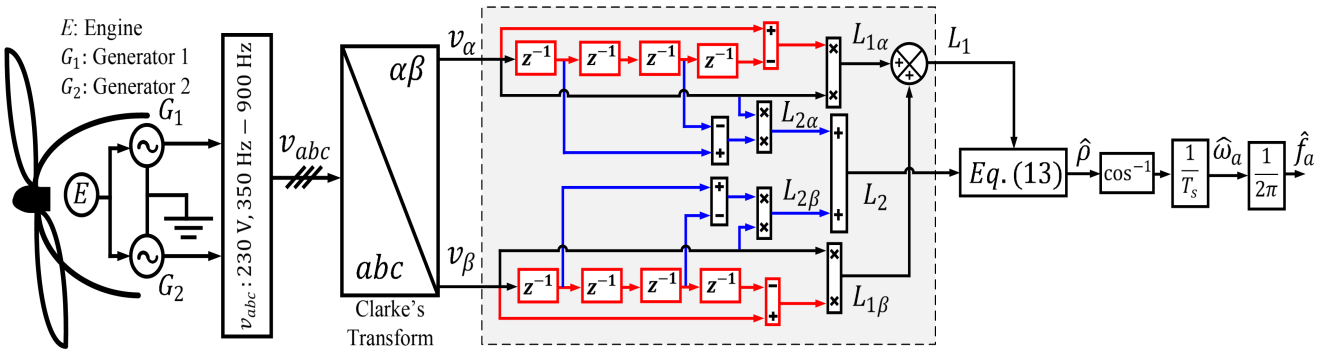

Figure 1: General block diagram of the proposed frequency estimator for a three-phase power system network of an electric aircraft.

where, $\xi > 0$ is a constant gain parameter and the estimated frequency is expressed as follows:

$$\hat{f}_a = \frac{\arccos(\hat{\rho})}{2\pi T_s} \tag{14}$$

The non-linear regression parameter ($\theta(t)$) abides by the persistently excitation property provided that $T_s < \pi/\omega_a$ [30]. The exponential convergence of (13) can consequently be ensured for the determination of fundamental frequency. This signifies that, for a low fixed sampling frequency condition, the selection of the control parameter ξ will affect the convergence speed and noise rejection abilities of the proposed frequency estimator. After performing extensive simulation exercises, it is, therefore, possible to conclude that $\xi = 1.6 * \bar{f}_a$ (where $\bar{f}_a = 625$ Hz is the mean value in the range [300 Hz, 950 Hz]) could be a suitable choice when the grid frequency varies within a range of 300 Hz to 950 Hz. Further, it is not stringent to adopt the recommended tuning gain parameter, since a designer can possibly try other methods to enhance the robustness as per the choice of application. Also, the selection of the parameter ξ depends on the satisfactory disturbance rejection abilities and the dynamic response time. Therefore, it is important to state that a structurally simple and easy-to-tune frequency estimator is proposed as being suitable for real-time application. Fig. 2 shows the DC-offset rejection capability of the proposed frequency estimator. Note that the magnitude response plot

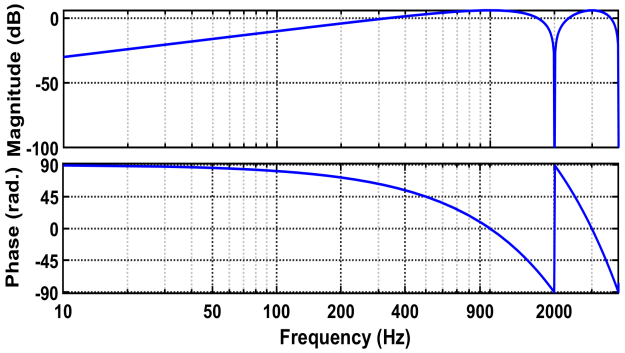

Figure 2: Magnitude and phase response plot of the proposed frequency estimator.

indicates that the proposed frequency estimator has a better immunity to the DC-offset component present in the grid signal. Furthermore, there are no issues concerning the ill-conditioning of the inverse trigonometric function, since L_1 and L_2 are the non-zero signals, as shown in Fig. 3. In order

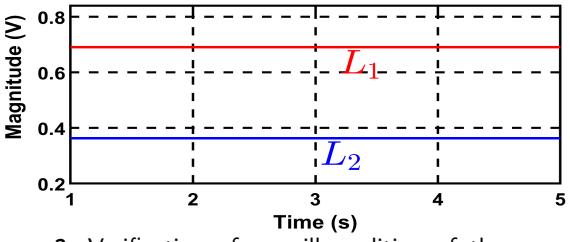

Figure 3: Verification of non ill-condition of the proposed frequency estimator.

to ensure that the discussion flows and remains compelling, the following section shows experimental results, thus making it possible to evaluate the potential of the proposed frequency estimator under adverse grid conditions.

3. Experimental Results and Discussion

The proposed five consecutive sample-(FCSs) based frequency estimator and the nonlinear FLL (N-FLL) [31] were simulated in a MATLAB/ Simulink environment. The tuning parameters for N-FLL were the following: Γ=0.02, K_a=1, γ_1^*=1 and σ_0=0.001, considering a rapid dynamic response. Using a sampling frequency (f_s=1/T_s) of 8 kHz, the algorithms are compiled and uploaded to a dSPACE real-time (DS1104) controller (see Fig. 4). The three-phase grid

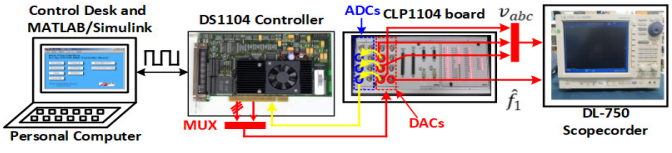

Figure 4: Experimental Setup.

voltage signal measured (1 p.u., 400 Hz) was generated internally and sent to the control algorithm. The results were then obtained using a 16 channel DL750 scopecorder. The

seven critical test cases considered in order to evaluate the dynamic performance of the proposed frequency estimator under adverse grid voltage conditions were the following:

1. **Unequal DC-offset in the grid signal:** The grid voltage signal at 400 Hz carries an unequal DC-offset component in 'a', 'b' and 'c' phases, i.e. 0.1 p.u., 0.2 p.u. and 0.3 p.u., respectively. Note that the N–FLL oscillates as shown in Fig. 5. However, the proposed FCS technique is able to accurately track the frequency information in 1 ms.

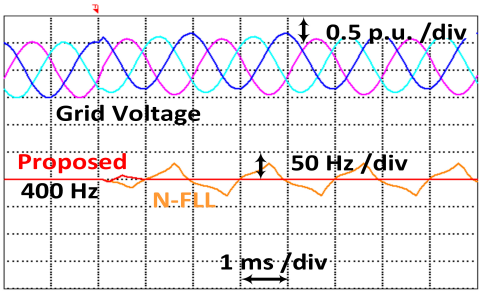

Figure 5: Frequency estimation in the presence of unequal DC-offset.

2. **50% symmetrical voltage sag:** In the event of a voltage sag, the proposed frequency estimator is sensitive to a sudden change in the fundamental amplitude, thus yielding a smaller overshoot in frequency when compared to N–FLL, as shown in Fig. 6.

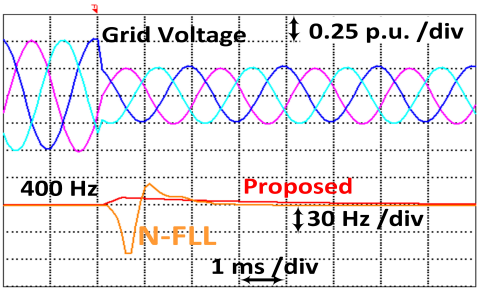

Figure 6: 50% symmetrical voltage sag.

3. **Phase angle jump of 40°:** All the phases of the grid voltage signal are rotated by 40°, as shown in Fig. 7. It is worth mentioning that the proposed FCS estimator has a similar kind of sensitivity to phase jump and voltage sag. However, both the frequency estimators can estimate the frequency without any steady-state error.

4. **10 dB Gaussian white noise immunity and frequency step (400-450 Hz):** The grid voltage signal is subjected to a 10 dB white noise along with a +50 Hz frequency step from 400 Hz, as shown in Fig. 8. Note that both schemes are capable of tracking the frequency step in the presence of noise. The FCS estimator is ≈2 ms faster than the N–FLL without any overshoot in the estimated frequency.

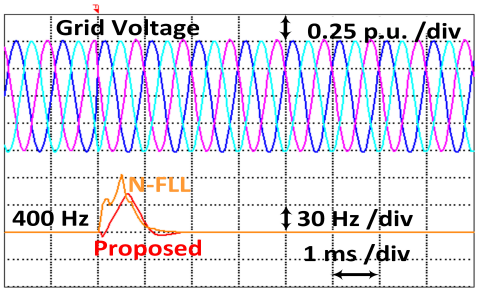

Figure 7: Frequency tracking performance in the presence of phase jump.

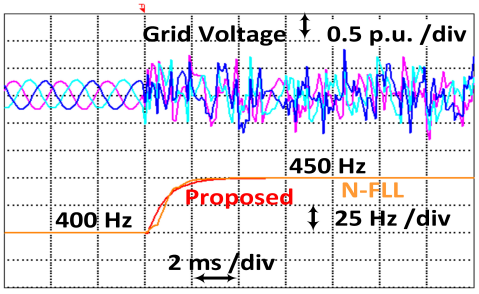

Figure 8: White noise and frequency step (400-450 Hz).

5. **Frequency step of 350-700 Hz:** As Fig. 9 shows, both schemes are capable of accurately tracking the large frequency step of +350 Hz from 350 Hz. It is worth noting that a good convergence to the steady-state value and stability are observable for both the estimators.

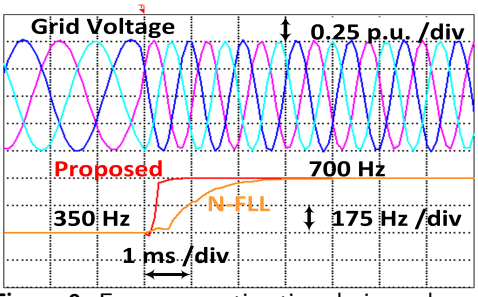

Figure 9: Frequency estimation during a large step of +350 Hz from 350 Hz.

6. **Grid voltage unbalance and frequency step of 350-900 Hz:** In Fig. 10, the phase 'a' magnitude is reduced to 0.1 p.u. in order to induce a fundamental negative sequence (FNS) component of 0.3 p.u. in the grid voltage signal. Note that the N-FLL is incapable of reaching 900 Hz. The control horizon of the N-FLL, therefore, requires further research in order to enhance the frequency tacking ability in the range of 350-900 Hz. The proposed FCS technique does not have this difficulty.

Table 1
Comparison between FCS technique and N–FLL

	Grid Voltage Conditions											
Test Cases →	Unequal DC-offset		40° Jump		50% Sag		350-700 Hz		Noise Immunity		350-900 Hz	
Estimators →	N–FLL	FCS	N-FLL	FCS	N–FLL	FCS	N–FLL	FCS	N–FLL	FCS	N–FLL	FCS
f_{peak} (Hz)	NA	+5	+60	+40	+28	+10	0	0	High	High	NA	0
t_s (ms)	NA	1	2	2	≈4	≈4	3	1	4	4	NA	≈2

Table 2
Comparison of Various Estimation Schemes Applied to an Electric Aircraft

	DC-Offset Removal	Disturbance Rejection	Steady-State Error	Unbalance Immunity	Sampling Frequency (Hz)	Control Parameters	Overall Response Time
DFT-PLL [18]	-	good	√	√	8kHz	4	16 ms
SSLKF-PLL [22]	-	better	√	√	8 kHz	3	12 ms
AO [26]	×	better	√	√	40 kHz	3	40 ms
RDO-PLL [29]	√	better	√	√	80 kHz	3	30 ms
N-FLL [31]	×	better	×	√	40 kHz	4	4 ms
Proposed Scheme	√	better	×	√	8 kHz	2	4 ms

*×–No, √–Yes

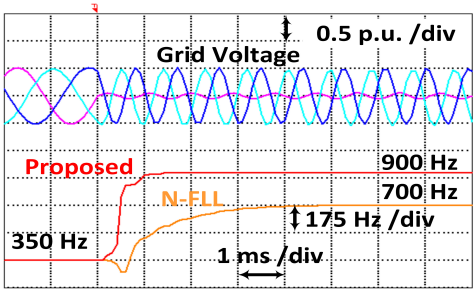

Figure 10: Large frequency step in the presence of FNS component.

Comparative Analysis of Hardware Results

Table 1 presents the peak errors observed in the frequency (f_{peak}) and setting time (t_s). Note that the FCS technique has a rapid dynamic response when compared to the N–FLL. Furthermore, the FCS technique undergoes fewer overshoots in the estimate of frequency when compared to N–FLL. However, the FCS technique can handle FNS and the DC-offset components present in the grid voltage signal. Moreover, no additional efforts are required in order to estimate the fundamental positive sequence component for the proper operation of the proposed frequency estimator. Also, once the sampling period is fixed, the proposed frequency estimator is dependent only on the choice of tuning gain parameter ξ whereas the N–FLL requires four tunig parameters, i.e. Γ, K_a, γ_1^*, and σ_0 [31]. This, therefore, confirms the simplicity of the proposed frequency estimator and its suitability for electric aircraft power systems.

Furthermore, Table 2 shows a comparison of the proposed scheme with other frequency estimation schemes, focusing on seven key features. Note that the proposed scheme and the RDO-PLL are immune to the DC-offset component present in the grid voltage signal when compared to the other schemes. Of all the schemes, the DFT-PLL slightly underperforms with regard to disturbance rejection abilities. Moreover, the N-FLL and the proposed scheme have a negligible amount of steady-state errors when compared to the other schemes. Nevertheless, all the estimation schemes have a good immunity to grid voltage unbalance. In addition, the overall dynamic performance of the proposed scheme is superior to that of the DFT-PLL, SSLKF-PLL, AO and RDO-PLL.

From the control viewpoint, it can be observed that the least count of control parameters associated with the proposed scheme indicates good control simplicity when compared to the existing solutions. Another key metric that may be important for a control algorithm is the choice of sampling frequency, which can affect the steady-state accuracy, transient response time and the cost of Digital/Analogue conversion units in the measurement section. It is notable that higher the sampling frequency, better is the accuracy, and vice-versa, as in the case of AO, RDO-PLL and N-FLL. Simultaneously, the higher number of samples in a fundamental cycle of a grid voltage signal can ensure the better stability of an algorithm.

On the other hand, the proposed algorithm is based on only five consecutive samples of the grid voltage signal, and a low sampling frequency of 8 kHz can, therefore, be adopted, similar to that which occurs in the case of DFT-PLL and SSLKF-PLL techniques,

without affecting the dynamic behaviour and steady-state accuracy. It is important to stress that the robustness of the proposed scheme in the presence of higher order harmonics is not verified in the current proposal. It is suggested that the incorporation of a fast responding pre-filtering solution would lead to better robustness to harmonics while maintaining a better dynamic response in order to compete with the conventional schemes. The proposed frequency estimator can, therefore, withstand the majority of gird voltage disturbances while ensuring a faster transient response time of 4 ms when compared to the well-known PLL techniques (DFT-PLL, SSLKF-PLL) and the improved PLL solutions (RDO-PLL).

4. Conclusion

A simple and efficient digital signal processing technique based three-phase fundamental frequency estimator is reported in this article. The storage of only five consecutive samples of the grid voltage signal accurately estimates the fundamental frequency information within 4 ms without any steady-state errors. Unlike the known frequency estimators employed for three-phase application, the FCS technique can handle the negative effects of the unequal DC-offset and FNS components present in the grid voltage signal. Another attractive feature of the proposed algorithm is its low sampling frequency operation, which makes it suitable for low-cost real-time controllers, as a consequence of which costly real-time embedded controllers can be replaced with cheaper microcontrollers. The prominent features of the proposed algorithm are summarized as follows:

- Pre-knowledge of the grid voltage disturbance is not required.
- It ensures better accuracy and resolution even with a low sampling frequency operation.
- The tuning efforts required are simpler owing to the reduced number of tuning gain parameters.
- There is a better immunity to unequal DC-offset and unbalance occurring in the grid voltage signal.
- Fast and stable dynamic behaviour under large frequency variations.

A. Intermediate Signals

The working principle of the proposed frequency estimator relies on the delayed signals which are generalized as follows:

$$v_{\alpha_L} = v_\alpha(k-L) = A_1 \cos(k\omega_a T_s - L\omega_a T_s) \tag{15}$$

$$v_{\beta_L} = v_\beta(k-L) = A_1 \sin(k\omega_a T_s - L\omega_a T_s) \tag{16}$$

where, L is the distance between the consecutive samples and $L \subset I^+$. For $L = 1, 3, 4$, the following intermediate signals can be obtained, as expressed below:

$$v_\alpha(k-1) = A_1 \cos(k\omega_a T_s - \omega_a T_s) \tag{17}$$

$$v_\alpha(k-3) = A_1 \cos(k\omega_a T_s - 3\omega_a T_s) \tag{18}$$

$$v_\alpha(k-4) = A_1 \cos(k\omega_a T_s - 4\omega_a T_s) \tag{19}$$

$$v_\beta(k-1) = A_1 \sin(k\omega_a T_s - \omega_a T_s) \tag{20}$$

$$v_\beta(k-3) = A_1 \sin(k\omega_a T_s - 3\omega_a T_s) \tag{21}$$

$$v_\beta(k-4) = A_1 \sin(k\omega_a T_s - 4\omega_a T_s) \tag{22}$$

For the sake of simplicity, the initial phase is assumed to be zero ($\phi = 0$) and the fundamental amplitude is assumed to be unity ($A_1 = 1$). It is clear that the proposed algorithm relies on the product of the grid voltage samples, and the generalized equations can, therefore, be obtained as follows:

$$v_\alpha(k) * v_\alpha(k-L) = \cos^2(k\omega_a T_s)\cos(L\,\omega_a T_s) + \sin(L\,\omega_a T_s)\sin(k\omega_a T_s)\cos(k\omega_a T_s) \tag{23}$$

The same approach can be applied to the β- axis component as follows:

$$v_\beta(k) * v_\beta(k-L) = \sin^2(k\omega_a T_s)\cos(L\,\omega_a T_s) - \sin(L\,\omega_a T_s)\sin(k\omega_a T_s)\cos(k\omega_a T_s) \tag{24}$$

The sum of (23) and (24) yields the following relationship:

$$v_\alpha(k) * v_{\alpha_L} + v_\beta(k) * v_{\beta_L} = \cos(L\,\omega_a T_s) \tag{25}$$

The intermediate signals expressed in (5) and (7) are re-written as follows:

$$L_{1\alpha} = v_\alpha^2(k) - \overbrace{v_\alpha(k)\,v_\alpha(k-4)}^{\text{Product with } L=4} \tag{26}$$

$$L_{1\beta} = v_\beta^2(k) - v_\beta(k)\,v_\beta(k-4) \tag{27}$$

When using (25) while considering $L = 4$, the sum of equations (26) and (27) yields the intermediate signal expressed below:

$$L_1 = L_{1\alpha} + L_{1\beta} = 1 - \cos(4\omega_a T_s) \tag{28}$$

where, $v_\alpha^2 + v_\beta^2 = 1$. Furthermore, the intermediate signals in equations (6) and (8) are re-written as follows:

$$L_{2\alpha} = \overbrace{v_\alpha(k)\,v_\alpha(k-1)}^{\text{Product with } L=1} - \overbrace{v_\alpha(k)\,v_\alpha(k-3)}^{\text{Product with } L=3} \tag{29}$$

$$L_{2\beta} = v_\beta(k)\,v_\beta(k-1) - v_\beta(k)\,v_\beta(k-3) \tag{30}$$

The sum of the equations (29) and (30) yields an intermediate signal,

$$L_2 = L_{2\alpha} + L_{2\beta} = \cos\omega_a T_s - \cos 3\omega_a T_s \tag{31}$$

If the trigonometric identities mentioned below are now applied to equations (28) and (31),

$$\cos(A) - \cos(B) = -2\sin(\frac{A+B}{2})\sin(\frac{A-B}{2}) \quad (32)$$

$$\cos(2A) = 2\cos^2(A) - 1 = 1 - 2\sin^2(A) \quad (33)$$

After simplifying the equations (28) and (31), a ratio can be obtained:

$$\frac{L_1}{L_2} = \frac{\sin(2\omega_a T_s)}{\sin(\omega_a T_s)} = 2\cos(\omega_a T_s) \quad (34)$$

The proposed frequency estimation law can, therefore, be easily formulated as discussed in (11).

References

[1] A. Griffo and J. Wang, "Modeling and Stability Analysis of Hybrid Power Systems for the More Electric Aircraft," *Elec. Power Sys. Res.*, vol. 82, no. 1, pp. 59–67, Jan. 2012.

[2] Y. Jia and K. Rajashekara, "An Induction Generator-Based AC/DC Hybrid Electric Power Generation System for More Electric Aircraft," *IEEE Trans. on Indus. Appl.*, vol. 53, no. 3, pp. 2485–2494, May-Jun. 2017.

[3] G. Buticchi, D. Barater, L. F. Costa, and M. Liserre, "A PV-inspired Low-Common-Mode Dual-Active-Bridge Converter for Aerospace Applications," *IEEE Trans. on Power Electron.*, vol. 33, no. 12, pp. 10467–10477, Dec. 2018.

[4] A. Barzkar and M. Ghassemi, "Electric Power Systems in More and All Electric Aircraft: A Review," *IEEE Access*, vol. 8, pp. 169314–169332, Sep. 2020.

[5] Z. Hao, X. Wang and X. Cao, "Harmonic Control for Variable-Frequency Aviation Power System Based on Three-Level NPC Converter," *IEEE Access*, vol. 8, pp. 132775-132785, 2020.

[6] S. Golestan, J. M. Guerrero, and J. C. Vasquez, "Three-Phase PLLs: A Review of Recent Advances," *IEEE Trans. on Power Electron.*, vol. 32, no. 3, pp. 1894–1907, Mar. 2017.

[7] F. Cupertino, L. Salvatore, E. Lavopa, M. Sumner and P. Zanchetta, "A DFT-based phase locked loop for phase and amplitude tracking in aircraft electrical systems," 2009 IEEE International Electric Machines and Drives Conference, 2009, pp. 1820-1825, doi: 10.1109/IEMDC.2009.5075450.

[8] F. D. Freijedo, J. Doval-Gandoy, O. Lopez, and E. Acha, "Tuning of Phase-Locked Loops for Power Converters Under Distorted Utility Conditions," *IEEE Trans. on Ind. Appl.*, vol. vol. 45, no. 6, pp. 2039–2047, Nov./Dec. 2009.

[9] H. Ahmed, S. Amamra, and M. Bierhoff, "Frequency-Locked Loop-Based Estimation of Single-Phase Grid Voltage Parameters," *IEEE Trans. on Ind. Electron.*, vol. 66, no. 11, pp. 8856–8859, Nov. 2019.

[10] *Voltage Characteristics of Electricity Supplied by Public Distribution Systems*, Eur. Std. EN–50160, 2008.

[11] S. Golestan, M. Monfared, F. D. Freijedo, and J. M. Guerrero, "Advantages and Challenges of a Type-3 PLL," *IEEE Trans. on Power Electron.*, vol. 28, no. 11, pp. 4985–4997, Nov. 2013.

[12] F. Gonzalez-Espin, E. Figueres, and G. Garcera, "An Adaptive Synchronous-Reference-Frame Phase-Locked Loop for Power Quality Improvement in a Polluted Utility Grid," *IEEE Trans. on Indus. Electron.*, vol. 59, no. 6, pp. 2718–2731, Jun. 2012.

[13] A. K. Verma, R. K. Jarial, P. R.-Sánchez, U. M. Rao, and J. M. Guerrero, "An Improved Hybrid Pre-Filtered Open-Loop Algorithm for Three-Phase Grid Synchronization," *IEEE Trans. on Ind. Electron.*, vol. 68, no. 3, pp. 2480–2490, Mar. 2021.

[14] S. Golestan, J.M. Guerrero, and J. C. Vasquez, "Steady-state linear Kalman filter-based PLLs for power applications: A second look," *IEEE Trans. Ind. Electron.*, vol. 65, no. 12, pp. 9795–9800, Dec. 2018.

[15] W. V. Lyon, *The Transient Analysis of Alternating-Current Machinery*. New York, NY, USA: Wiley, 1954.

[16] M. Mirhosseini, J. Pou, V. G. Agelidis, E. Robles, and S. Ceballos, "A Three-Phase Frequency-Adaptive Phase-Locked Loop for Independent Single-Phase Operation," *IEEE Trans. on Power Electron.*, vol. 29, no. 12, pp. 6255–6259, Dec. 2014.

[17] S. Gautam, Y. Lu, W. Hassan, W. Xiao, and D. D.-C. Lu, "Single Phase NTD PLL for Fast Dynamic Response and Operational Robustness Under Abnormal Grid Condition," *Electr. Power Syst. Res.*, vol. 180, Mar. 2020.

[18] E. Lavopa, P. Zanchetta, M. Sumner, and F. Cupertino, "Real-Time Estimation of Fundamental Frequency and Harmonics for Active Shunt Power Filters in Aircraft Electrical Systems," *IEEE Trans. on Indus. Electron.*, vol. 56, no. 8, pp. 2875–2884, Aug. 2009.

[19] J. F. Guerreiro, J. A. Pomilio, and T. Davi Curi Busarello, "Design and Implementation of a Multilevel Active Power Filter for More Electric Aircraft Variable Frequency Systems," *Brazilian Power Electron. Conf.*, Gramado, Brazil, 2013, pp. 1001–1007.

[20] A. Bellini, S. Bifaretti, and S. Costantini, "A PLL-based filter for speed noise reduction in drives using a resolver transducer," *in Proc. IEEE Int. Symp. Ind. Electron.*, vol. 2, pp. 529–534, 2002.

[21] A. Bellini and S. Bifaretti, "Performances of a PLL based digital filter for double-conversion UPS," *in Proc. 13th Int. Power Electron. Motion Control Conf.*, 2008, pp. 490–497.

[22] S. Bifaretti, P. Zanchetta, and E. Lavopa, "Comparison of two three-phase PLL systems for more electric aircraft converters," *IEEE Trans. Power Electron.*, vol. 29, no. 12, pp. 6810–6820, Dec. 2014.

[23] Ž. Zečević, B. Krstajić, and T.Popović, "Improved frequency estimation in unbalanced three-phase power system using coupled orthogonal constant modulus algorithm," *IEEE Trans. Power Del.*, vol. 32, no. 4, pp. 1809–1816, Aug. 2017.

[24] H. Yang, Y. Zhang, J. Liang, J. Gao, P. D. Walker, and N. Zhang, "Sliding mode observer based voltage-sensorless model predictive power control of PWM rectifier under unbalanced grid conditions," *IEEE Trans. Ind. Electron.*, vol. 65, no. 7, pp. 5550–5560, Jul. 2018.

[25] Z. Dai, S. Lv, J. K. Mwaniki, and J. Zhang, "Global accurate estimation of positive- and negative-sequence voltage components for variable frequency AC systems," *IET Power Electron.*, vol. 11, no. 10, pp. 1730–1737, Aug. 2018.

[26] Z. Dai, J. Yang, D. Rao, J. Zhang, and Z. Zhang, "A global convergence estimator of grid voltage parameters for more electric aircraft," *IEEE Trans. Ind. Electron.*, vol. 67, no. 9, pp. 7540–7549, Sep. 2020.

[27] M. Tang, S. Bifaretti, S. Pipolo, A. Formentini, S. Odhano, and P. Zanchetta, "Disturbance rejection ability enhancement using repetitive observer in phase-locked loop for more electric aircraft," *in Proc. IEEE Energy Convers. Congr. Expo.*, 2020, pp. 6379–6384.

[28] M. Tang, A. Formentini, S. A. Odhano, and P. Zanchetta, "Torque ripple reduction of PMSMs using a novel angle-based repetitive observer," *IEEE Trans. Ind. Electron.*, vol. 67, no. 4, pp. 2689–2699, Apr. 2019.

[29] M. Tang, S. Bifaretti, S. Pipolo, A. Formentini, S. Odhano and P. Zanchetta, “A Novel Low Computational Burden Dual-Observer Phase-Locked Loop With Strong Disturbance Rejection Capability for More Electric Aircraft," *IEEE Trans. Indus. Appl.*, vol. 57, no. 4, pp. 3832–3841, July–Aug. 2021.

[30] P. A. Ioannou and J. Sun, *Robust adaptive control. Courier Corporation, 2012.*

[31] Z. Dai, M. Fan, H. Nie, J. Zhang, and J. Li, “A Robust Frequency Estimation Method for Aircraft Grids Under Distorted Conditions," *IEEE Trans. Indus. Electron.*, vol. 67, no. 5, pp. 4254–4258, May 2020.